Modular Foldable Surfaces: a Novel Approach Based on Spatial Mechanisms and Thin Shells

Yuchen Wei* and Sergio Pellegrino†

California Institute of Technology, Pasadena, CA 91125, USA

This paper investigates a set of novel techniques that lead to modular, deployable surface arrays which could be either flat or curved in their deployed shape. The two components of the proposed concepts are thin shells with smooth folds and spatial mechanisms with rolling hinges. Kinematics of the mechanism and motion of the shell has been shown to be fully compatible with each other during folding and unfolding. This basic module is then articulated to create multiple modular tessellations, which form a series of foldable surfaces. We further demonstrate that curvature could be introduced to the initially flat shells using bonded piezoceramic actuators. The techniques and concepts proposed in this paper could be valuable for the design of future deployable space-based telescope and other reflective arrays which require high shape precision with low storage area and volume.

Nomenclature

A_i	Coordinate transformation matrix at i^{th} hinge
d	Hinge line separation
d'	Panel separation distance in folded configuration
D	Shell bending stiffness
DOF	Degree of freedom
M	Mobility of mechanism
t	Shell thickness
W	Crease region width
α	Ratio between crease width and hinge line separation
β	Bending stiffness ratio between panel and crease

I. Introduction

Large, precision reflectors composed of rigid panels in space have many applications, including telescope mirrors, solar concentrators and antennas, but so far only few studies have addressed the challenges of packaging and deployment of such structures. Studies of rigid-surface antennas and reflectors consisting of rigid petals that wrap around a central hub have been carried out in the 1980's and 1990's, examples include the TRW Sunflower,[1] the Dornier/ESA FIRST antenna,[2] the Cambridge Solid Surface Deployable Antenna (SSDA),[3] and the deployable telescope mirror concept by Lake et al.[4] However, their structural complexity and high areal density have been an obstacle to further development; also, there are fundamental difficulties in scaling up or tessellating these concepts. Similar concepts have recently been adopted for small satellite applications.[5,6] The pull from the application side has resulted in recent studies on alternative approaches, for example the robotic assembly of a giant, 100 m diameter, telescope proposed by Lee, et al.[7] based on identical deployable truss modules; and several proposals of deployable annular space telescope concepts based on tensegrity and pantograph structures, including a 30-m space based observatory by Rey et al.[8] and a 20 m diameter annular mirror by Durand et al.[9]

*Ph.D Candidate, Graduate Aerospace Laboratories, 1200 E California Blvd MC 205-45.

†Joyce and Kent Kresa Professor of Aeronautics and Professor of Civil Engineering; Jet Propulsion Laboratory Senior Research Scientist, Graduate Aerospace Laboratories, 1200 E California Blvd MC 105-50, AIAA Fellow.

We are interested in developing modular deployable structures solutions that exploit the properties of regular tessellations emerging from recent research on packaging techniques from rigid-foldable origami. Tachi[10] presented solutions for designing rigid-foldable structures based on triangular and quadrilateral mesh. Chen[11] has proposed a systematic solution based on spatial mechanisms for thick rigid panels connected by hinges of zero width. Because the solution is based on rigid origami, foldability into a tight package is achieved without incurring any deformation of the panels.

Parallel advances in manufacturing and shape control of thin shell mirrors have provided another new direction that can support this approach. Reflectors made from carbon-fiber composite rollable thin shells have been proposed[12–14] to store the reflector compactly. Patterson[15] and Steeves[16] have developed deformable thin mirror technologies based on active laminates consisting of thin shell substrates and active layers.

In this paper we propose a new concept for flat, thin shell mirrors that can be elastically folded using a simple four-panel pattern inspired by origami. We then develop design techniques to integrate the mirrors with modular spatial mechanisms that stabilize the mirrors during folding and hold them in the deployed configuration, and also demonstrate that after deployment the mirrors can be deformed into spherical caps by means of surface-mounted piezoceramic actuators. Lastly, we propose tessellation concepts to form assemblies of these mechanism-supported mirrors.

The mirrors are made of a carbon fiber composite with embedded elastically foldable regions made of metallic glass. A four-bar spatial mechanism with rolling hinges supports each mirror along the outer edge. The fold pattern of the mirror matches the kinematics of the mechanism, and hence when the mirror is folded its bending deformation is concentrated in the fold regions, thus avoid introducing high strains in the mirror panels. These features make the proposed concepts attractive for the design of primary mirrors for future space telescopes.[16,17]

The paper is organized as follows. We first introduce the methodology for integrating creased thin shells and spatial mechanisms. We then introduce the chosen spatial mechanism, and present the development of a compactly foldable spatial mechanism based on rolling hinges. A parametric analysis of this mechanism is presented and its kinematics are analyzed numerically. These results lead to a specific design for a foldable thin shell that is attached to a mechanism and the folding characteristics of the shell-mechanism are evaluated by means of a detailed finite element analysis. A description of a physical prototype of this concept is presented, and of the folding tests that were performed. Next, several tessellation concepts are introduced. Finally, an experimental demonstration shows that the curvature required for an application requiring curved mirrors with relatively short focal length can be introduced in the shell, in the deployed configuration, by means of a piezoceramic layer bonded to the back surface of the shell.

II. Attaching a Flat Thin Shell to Articulated Rigid Links

We consider the problem of attaching a rectangular thin shell with an elastic fold of width w, to a simple mechanism, consisting of a pair of rigid links connected by revolute joints that are rotated by an angle γ. The fold region of the shell has lower bending stiffness; whereas the rest of the shell is thicker. The shell is fixed along the edge to the mechanism, except for the fold region.

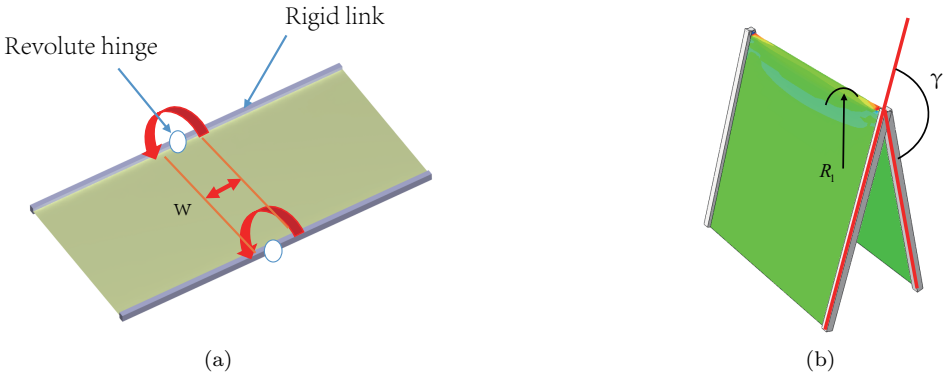

Figure 1. Thin shell attached to a mechanism (a) flat and unstressed and (b) folded. Red region denotes the ridge singularity.

A. Avoiding Ridge Singularity in the Folded Shell

A "ridge singularity" will appear along the fold line when the hinges of the mechanism are rotated, Figure 1. This problem is well studied and understood,[18] and it can be shown that:

$$R_1 \sim t^{1/3} w^{2/3} \gamma^{-4/3} \tag{1}$$

where R_1 is the fold radius, and t, w are the thickness and width of the crease region of the shell, and α is the dihedral angle. Note that R_1 tends to be singular as $w \to 0$ and $\gamma \to \pi$, which are the common assumptions in conventional origami studies. The induced strain in the fold region will cause local buckling, plastic deformation or even material failure.

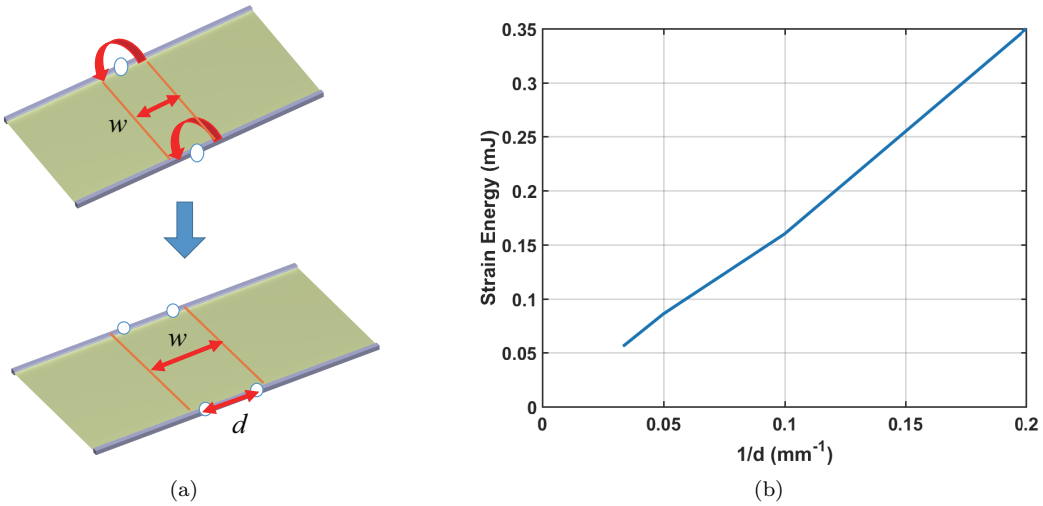

(a) (b)

Figure 2. (a) Introduction of hinge separation in folded thin shell attached to rigid link assembly. (b) Bending energy of shell scales inversely with crease width.

An easy way to eliminate the ridge singularity is by separating the hinge lines in the mechanism, to better match the kinematics of the mechanism to the deformation of the elastic shell. The width of the fold region is also increased, as shown in Figure 2 and discussed in detail in the next section. In effect, this doubles the number of hinges, as a pair of hinges can better accommodate a smooth transition in the shell during folding. Moreover, it decreases the strain energy stored in the shell, as shown in Figure 2(b), by almost eliminating the bending deformation away from the fold region of the shell. This property is key to the integration of foldable thin shells to spatial mechanisms.

B. Influence of Fold Width and Bending Stiffness on Folded Shape

A parametric study of the influence of the crease region width and bending stiffness on the folded shape, shown in Figure 3, was carried out. The goal was to minimize the separation distance between the panels on either side of the folded shell. In all these studies: 1) the shell was only partially supported along the edges (indicated by the black lines in the figure); 2) the width of the fold region was set to be $w = \pi/2 \times d$.

The results are presented in Figure 3, which shows that when the stiffness ratio β drops below 0.1, the normalized separation distance d' is very close to the hinge line separation d. From numerical simulations, $d' \propto (\beta)^3$. This result will be used for the design of foldable shells in Section IV.

III. Modular Spatial Mechanism with Rolling Hinges

The mechanism concept proposed in this section was inspired by the Miura-Ori folding pattern.[19] The basic repeating unit of Miura-Ori is the symmetric degree-4 vertices pattern shown in Figure 4. It is kinematically equivalent to a four bar spherical mechanism, and hence possesses one degree of freedom. This can be shown by replacing the zero-width crease lines with revolute joints, and then noting that the four hinge lines intersect at a point throughout folding and deployment. Variations of this unit will lead to both the spatial mechanism and the foldable thin shell concept presented in the following section.

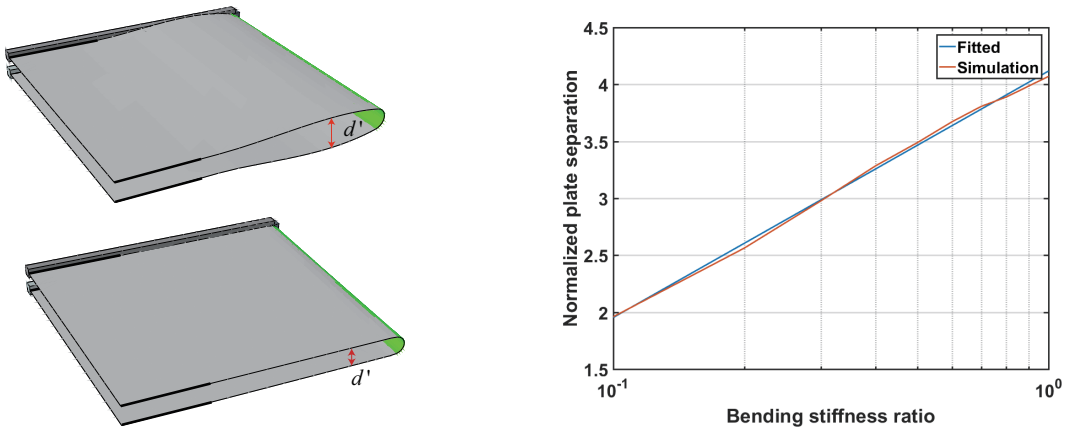

(a) (b)

Figure 3. Crease region bending ratio effect on shell separation distance in folded configuration. Results based on finite element simulations. Black line denotes the fixed position. The link at the front is hidden.

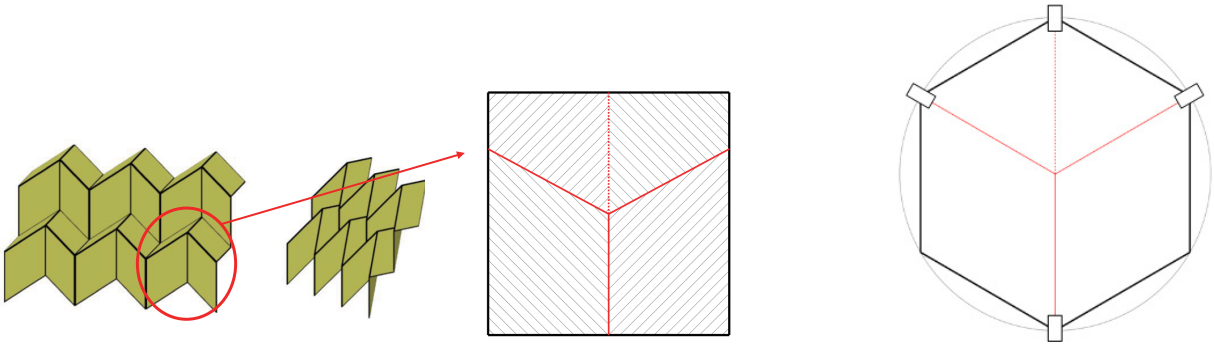

(a) (b)

Figure 4. (a) Miura-Ori pattern.[20] Red lines denote fold lines, shaded regions denote panels. (b) Spherical mechanism equivalent to repeating unit. Rectangles denote revolute joints.

A. Four Bar Spatial Mechanism

The main challenges in transforming the chosen origami pattern into a compactly foldable spatial mechanism are the need to accommodate the thickness of the structure and to preserve the single degree of freedom. Conventional revolute hinges will prevent the mechanism from being folded beyond the point of first self-contact between the linkages of the mechanism. To remove these constraints, the original single hinge was split into a pair of coupled revolute joints whose axes intersect at a common point, as shown in Figure 5. By introducing the rolling hinge pair both challenges are addressed.

A conventional rolling hinge is composed of two elements: a pair of curved contact surfaces and tensioned cables/bands.[22] The surface pairs are held in contact by the tensioned cables, to prevent sliding and thus providing a single DOF. This hinge is attractive for space applications due to its high stiffness, low friction and structural simplicity.[22] The profile of the contact surface can be designed to achieve different relative motions, e.g. multi-stability.[23] In this application, the contact surfaces are made conical to meet the requirement that in a spherical mechanism the hinge axes should intersect at a common point O. Kinematically, the relative motion of this modified rolling hinge pair is equivalent to a three-bar mechanism with mirror symmetry and common hinge axes intersection, as shown in Figure 6. In Figure 5 conical rolling hinge pairs were introduced to replace the revolute hinge pairs GF, ED, and CB. Joint A does not need to be replaced with a hinge pair because it does not close fully.

More importantly, these hinge pairs preserve the single degree of freedom of the original degree-4 vertices pattern. This can be shown by considering the modified Grubler-Kutzbach equation for the mobility of the

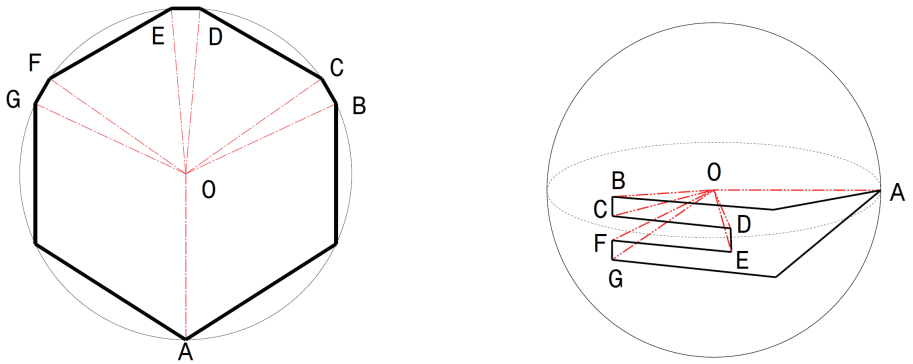

Figure 5. (a) Introduction of coupled revolute joints into the mechanism. b) Folded configuration of modified mechanism. All vertices rest on the same spherical surface.

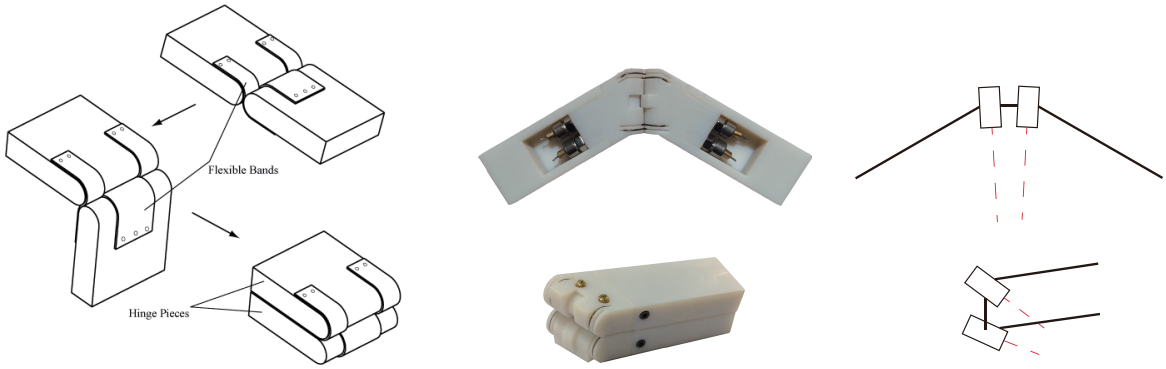

Figure 6. (a) Conventional rolling hinge with cylindrical contact surface pair. (b) Rolling hinge with conical contact surface pair. It is equivalent to a three-bar mechanism with angular symmetry constraint.

proposed spherical mechanism:

$$M = 3(n-1) - 2j - r \tag{2}$$

where $n = 7$ is the number of links, $j = 7$ the number of hinge lines, $r = 3$ the number of contact surface pairs. Here the mobility M is defined without considering the whole mechanism's rigid body motion in space, and examined in a coordinate system fixed to one element, e.g. bar AG. The position of each element can be determined by three independent parameters, normally the Euler angles. Both the revolute and rolling joint allows 1 DOF rotation between adjacent members of the mechanism, thus remove 2 DOF from M. Thus the mobility of mechanism in Figure 5 is reduced from:

$$M = 3(7-1) - 2 \times 7 - 0 = 4 \tag{3}$$

to the single DOF mechanism in Figure 5:

$$M = 3(7-1) - 2 \times 7 - 3 = 1 \tag{4}$$

The following sections will be based on use of this modified mechanism.

B. Kinematic Analysis of Spatial Mechanism

The kinematics of the proposed four-bar mechanism were studied by constructing the loop closure equation, using the Denavit-Hartenberg notation,[24] as shown in Figure 8. A 4 by 4 transformation matrix A_N converts the coordinates on hinge N to $N-1$ through the matrix multiplication:

$$p'_{N-1} = A_N p'_N \tag{5}$$

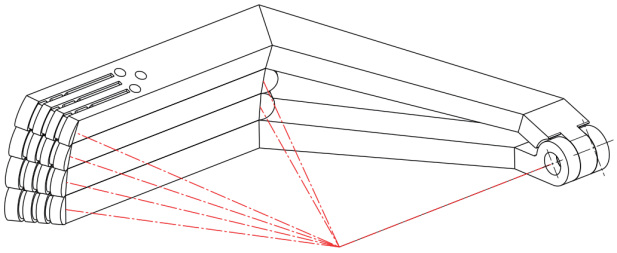

(a)

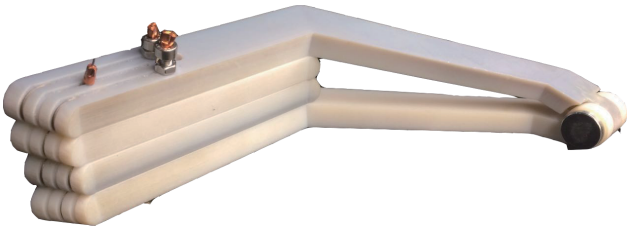

(b)

Figure 7. (a) Spatial mechanism with conical rolling hinges. Grooves on the surface hold the tension wires. (b) Folded configuration of 3D-printed mechanism prototype shows compact folding. Screws on the model are used to tension the cable.

where the matrix A_N has the structure:

$$A_N = \begin{bmatrix} \cos\theta_N & -\sin\theta_N \cos\alpha_N & \sin\theta_N \sin\alpha_N & a_N \cos\theta_N \\ \sin\theta_N & \cos\theta_N \cos\alpha_N & -\cos\theta_N \sin\alpha_N & a_N \sin\theta_N \\ 0 & \sin\alpha_N & \cos\alpha_N & r_N \\ 0 & 0 & 0 & 1 \end{bmatrix} \tag{6}$$

and its inverse is:

$$A_N^{-1} = \begin{bmatrix} \cos\theta_N & -\sin\theta_N & 0 & -a_N \\ -\sin\theta_N \cos\alpha_N & \cos\theta_N \cos\alpha_N & \sin\alpha_N & -r_N \sin\alpha_N \\ \sin\theta_N \sin\alpha_N & -\cos\theta_N \sin\alpha_N & \cos\alpha_N & -r_N \cos\alpha_N \\ 0 & 0 & 0 & 1 \end{bmatrix} \tag{7}$$

where, r_N is the adjacent joint displacement, a_N is the hinge axes normal distance, θ_N represents the displacement of each joint, and α_N is the twist angle between adjacent joints. For the mechanism studied here, $\alpha_N = 0$ (no twisting) and $a_N = 0$ since all hinge axes intersect at the common center.

The loop-closure condition can then be obtained by applying coordinate transformations sequentially around the links of the mechanism:[21]

$$A_1 A_2 A_3 A_4 A_5 A_6 A_7 = I \tag{8}$$

Note that the angles θ_N are the only variables that control the motion of the mechanism. Due to the symmetry of the rolling hinges and the symmetry of the mechanism, $\theta_4 = \theta_5 = \theta_1 = \theta_2$, and $\theta_6 = \theta_7$. Hence, the final expressions only contain θ_1, θ_3 and θ_6. The simplest form of the closure equation can be achieved by the transformation:

$$A_3 A_4 A_5 - A_2^{-1} A_1^{-1} A_7^{-1} A_6^{-1} = 0 \Rightarrow \begin{bmatrix} f_1(\theta_1,\theta_3,\theta_6) & f_2(\theta_1,\theta_3,\theta_6) & f_3(\theta_1,\theta_3,\theta_6) & 0 \\ f_4(\theta_1,\theta_3,\theta_6) & f_5(\theta_1,\theta_3,\theta_6) & f_6(\theta_1,\theta_3,\theta_6) & 0 \\ f_7(\theta_1,\theta_6) & f_8(\theta_1,\theta_6) & f_9(\theta_1,\theta_6) & 0 \\ 0 & 0 & 0 & 0 \end{bmatrix} = 0 \tag{9}$$

Here each entry is a 6^{th}-order transcendental equation and solving this system of equations numerically yields the angular input-output relation of the mechanism. Equation 9 also reveals the mechanism's single

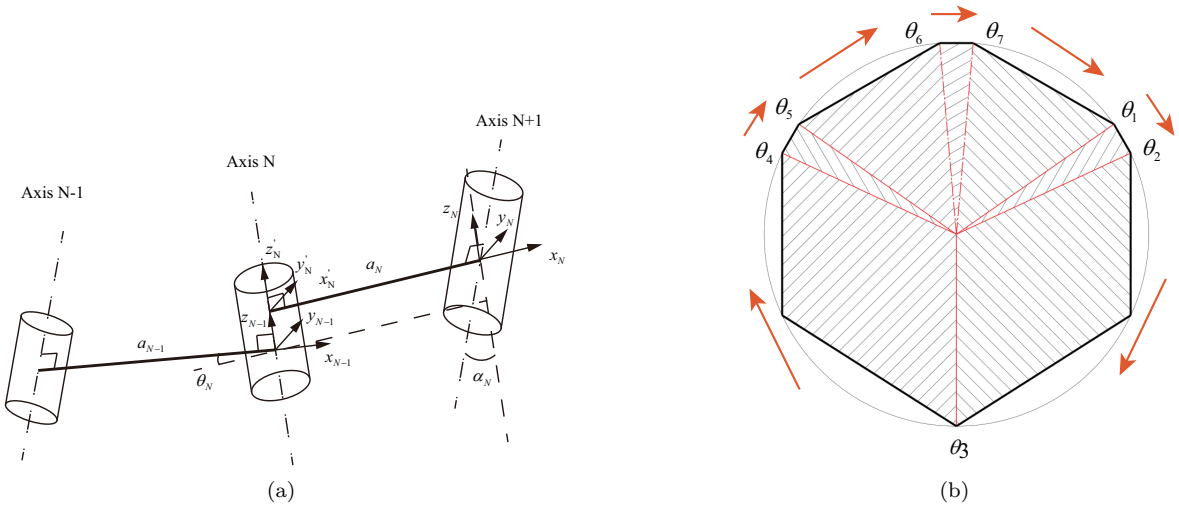

(a) (b)

Figure 8. (a) Denavit - Hartenberg notation of coordinate transformation (b) Arrows denote the sequence of coordinate transformations.

DOF nature: once the relation between θ_1 and θ_6 has been obtained by solving the third row, the value of θ_3 at each solution step can then be calculated from any entry of the first or second row.

These kinematic relations were solved using the Newton-Ralphson method. Taking θ_1 as the input angle, $\theta_1 \in [0, \pi/2]$, θ_3 and θ_6 can be calculated. The analysis procedure is illustrated in Figure 9.

It was found that the numerical solution is highly sensitive to the step size when the mechanism is in the flat configuration, i.e. when $\theta_1 = \theta_3 = \theta_6 = 0$. In this configuration, by decreasing the step size of the solver, the solution jumps to a different branch, as shown in Figure 10. This result indicates that the flat configuration is a bifurcation point for the kinematic path of the mechanism. Note that the numerical solution captures this behavior without any a priori knowledge. The second solution branch corresponds to the alternative (and less interesting) folded configuration shown in Figure 10.

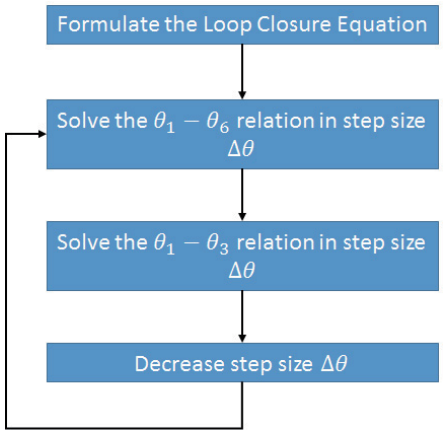

Figure 9. Solution procedure for loop closure equation.

IV. Integration of Thin Shell with Spatial Mechanism

This section presents the design, simulation and prototyping steps leading to a mechanism-supported foldable thin shell with finite width crease pattern, whose folding motion can be guided by the mechanism synthesized in Section III.B. The approach that leads to a smooth integration of the two structures is presented.

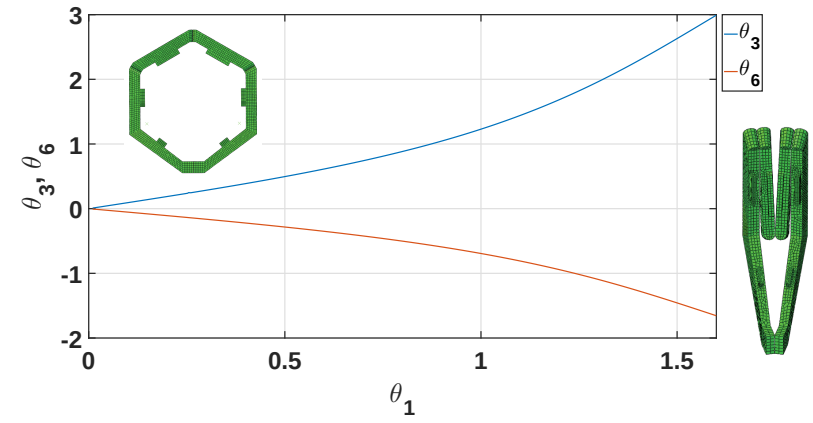

(a)

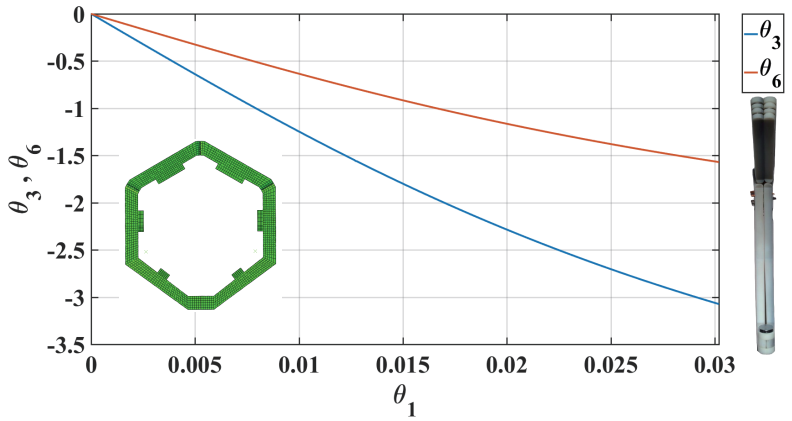

(b)

Figure 10. (a) Branch 1 of bifurcated solution to loop closure equation, corresponds to normal folded configuration. (b) Branch 2 corresponds to structure folding in half.

The starting point is the Miura-Ori derived folding pattern, trimmed along the edges to obtain a hexagonal shape. The mountain and valley folds are replaced with finite-width elastic folds. To guarantee a smooth integration with the mechanism (i.e. no significant changes in deformation are induced due to the integration of the two structures), a series of finite element analyses were performed.

A. Finite Element Model Description

The shell was modeled using S3R triangular shell elements in Abaqus/Explicit 6.14-5. Radius of the circumscribed circle of the shell is 125 mm, and the thickness of the panels is 150 μm . To capture the deformation of the fold region, the largest element size was decreased to 1.3 mm, compared to the 5.7 mm in the panels of the shell. The mechanism was modeled using C3D8 linear hexahedron elements, and each link is defined as a rigid body. Each rolling hinge was modeled as two revolute joints with intersecting hinge lines using the connector element CONN3D2, and their rotation angles were defined as identical throughout the folding process. Folding was imposed by prescribed rotations of the rolling hinges. To implement a quasi-static folding procedure in the explicit solver, the techniques described by Mallikarachchi[25] were implemented. The complete simulated folding sequence is shown in Figure 12.

B. Sensitivity of Shell Deformation to Fold Width Ratio

In the simulation, the bending stiffness ratio between panels and fold regions, β, was chosen as 90, based on the available material for the crease and the layup of the composite shell (more details are provided in

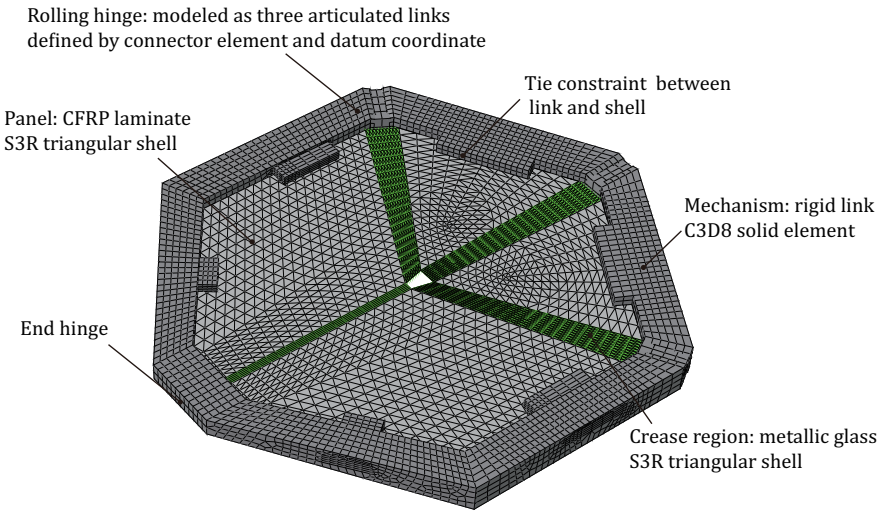

Figure 11. Finite element model of foldable thin shell with edge supported mechanism. Shell is perforated at the center to avoid singularity. Rolling hinge is modeled as three articulated hinges with equal angle constraint during folding.

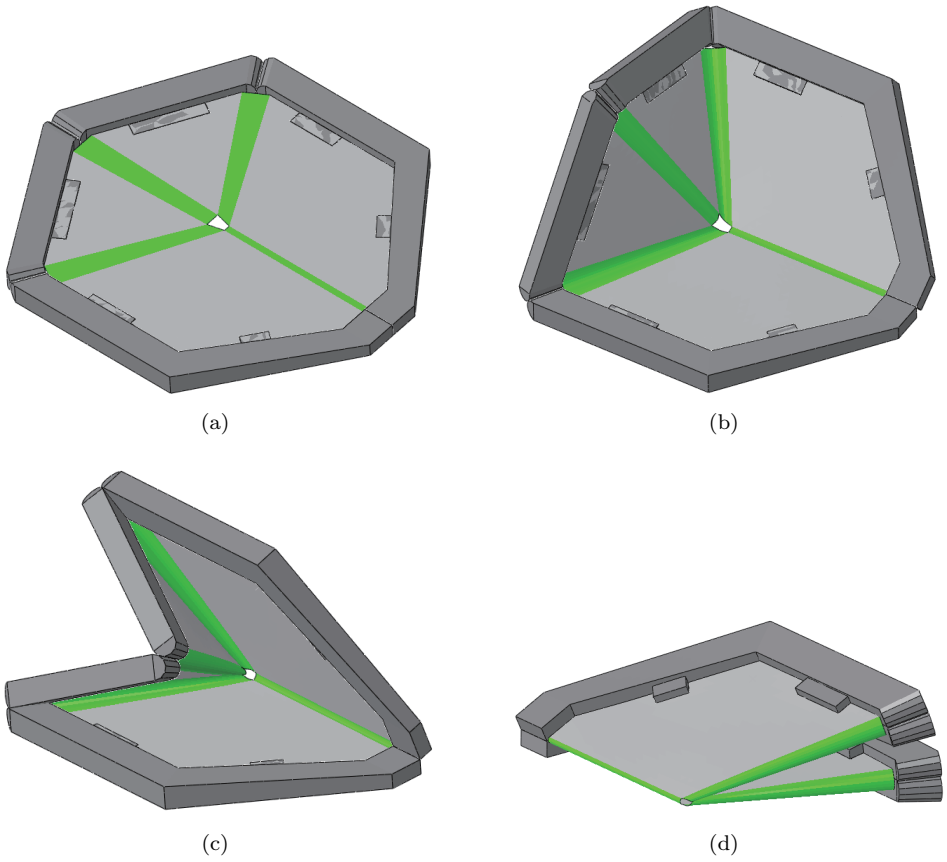

Figure 12. Folding sequence simulated in Abaqus/Explicit. Folding is driven by applying rotations to the connector elements that simulate the rolling hinges.

Section C). A series of simulations were performed with different width ratios for the fold region. It was found that for $\alpha < \pi/2$, significant out-of-plane panel deformation appears in the final folded configuration even for small values of β, as shown in Figure 13. This result guided the design of the physical prototype in

the next section.

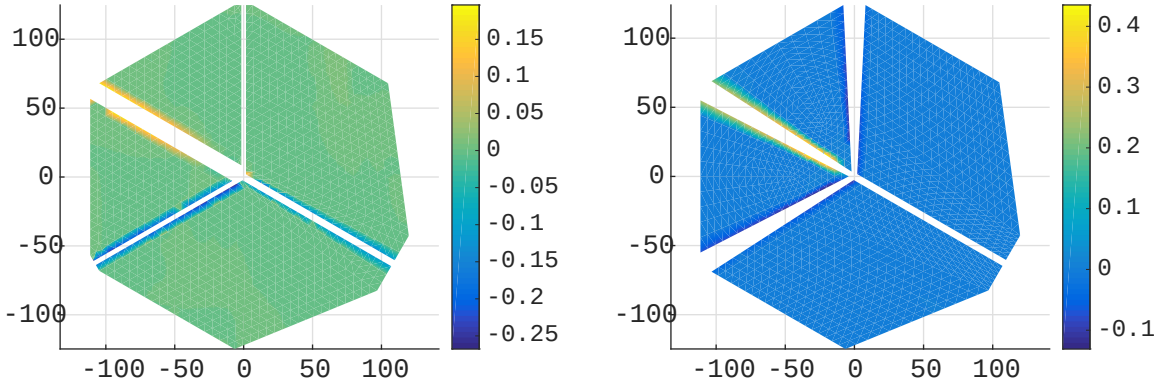

(a) (b)

Figure 13. Curvature of the panels in folded configurations, Unit in mm^{-1}. a) Local α smaller than $\pi/2$. b) Crease pattern of the final design, with $\alpha = \pi/2$ satisfied globally, and panel curvature is orders of magnitude lower compared with a).

C. Shell-Mechanism Prototype

A prototype of the mechanism-supported thin shell was built based on a design verified through the folding simulations. The thin shell consists of carbon fiber reinforced plastic (CFRP) unidirectional tape with a layup orientation of $[60°/120°/0°]_s$ and thickness of 150 μm. The tape contained M55J fibers impregnated with ThinPreg^{TM} 120EPHTg-1 epoxy. Thin amorphous metal sheet was used for the fold regions due to its high yield stress. The particular sheet used in the prototype is an iron-nickel based product from Metglas[26] with thickness of 24 μm. The whole laminate and metal sheet were cured together in an autoclave.

The prototype was folded by rotating the end joint, as shown in Figure 14. As predicted by the simulation, the shell panels stay flat during folding, and the whole shell remained intact after dozens of folding and deployment cycles.

V. Flat or Curved Tessellations of Multiple Modules

Larger structures can be obtained from a tessellation of the basic module created and demonstrated in the previous section. The deployment ratio is defined as the ratio between the radii of the spheres circumscribed to the vertices of the mechanism in the deployed and folded configurations.

As an example, the basic module is first tessellated into several symmetric assemblies, both flat and curved. All adjacent modules are connected through revolute joints. Folding of each concept was simulated with Abaqus/Explicit 6.14-5, using the same methods developed in Section IV. For simplicity, the shells were not included in the simulations. The rolling hinge pairs were modeled as three-bar mechanisms with equal angle constraints.

A. Tessellation of Hexagonal Modules based on Three-fold Symmetry

As a first example, the regular hexagonal modules are connected by revolute joints along the bars connected to the end hinge to create a flat tessellation. The axes of the hinges joining adjacent modules intersect at a common point O, which is separate from the common mid-surface of the bars. This configuration forms a 6-bar Bricard mechanism around the connected bars. The Bricard mechanism is well studied by You, etc.,[27] and has been shown to possess only 1 DOF. It can then be concluded that the whole tessellation also possesses a single DOF, since the folding and unfolding of each module can be driven by the rotation of the end hinge. This results is confirmed by the simulations shown in Figure 15 and Figure 16. The complete folding of the whole tessellation is driven by folding only one module.

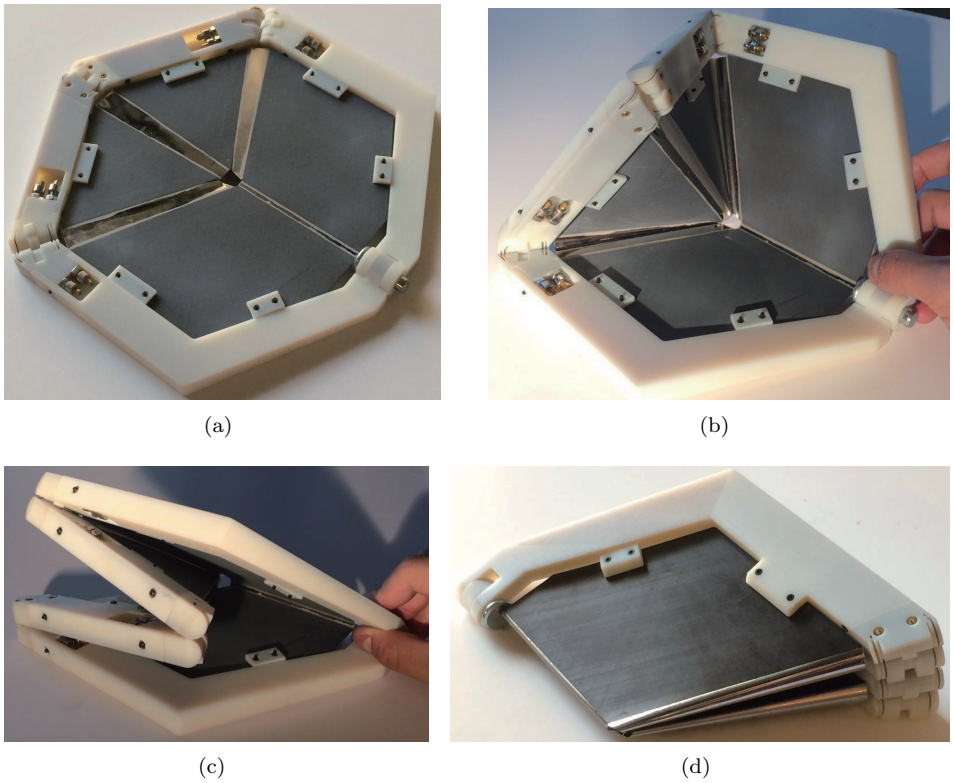

(a) (b) (c) (d)

Figure 14. Folding sequence of prototype. The whole sequence is driven solely by rotating the end hinge.

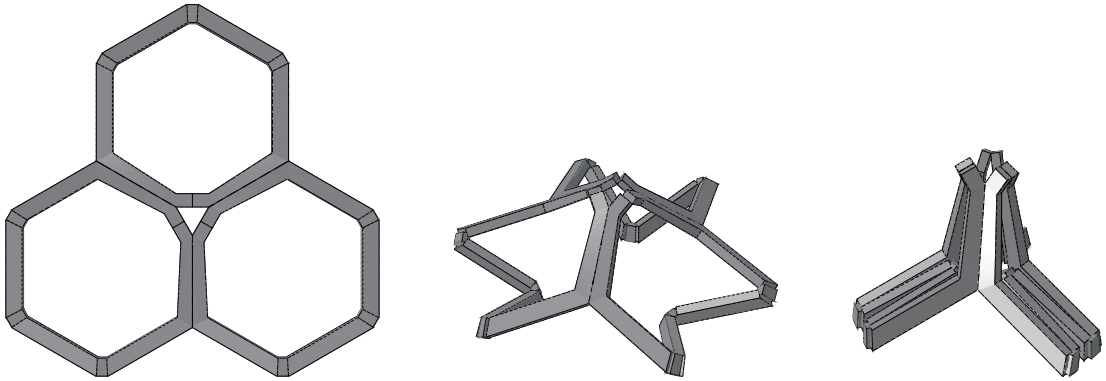

(a) (b) (c)

Figure 15. Three-fold symmetry tessellation concept with flat deployed configuration. b) and c) shows the half and fully folded state. This concept has a deployment ratio of 2.1. The subplots don't share the same scale.

To form a non-flat tessellation configuration with all the vertices resting on a spherical surface, small modifications are made to the original deployable module. The basic modules are no longer regular hexagons, due to the angular defect at the vertex of the tessellation. However, since each module still lies on a plane and remains symmetric, it can be shown that we only need to slightly shorten two sides; the module also remains foldable since the center part of the tessellation remains a 6-bar Bricard mechanism with angular defect. The deployment process is shown in Figure 16. The dihedral angle between adjacent hexagons is 38.975° . The deployment ratio could be further increased by detaching one of the inter-module hinge, however the mechanism no longer preserves a single DOF.

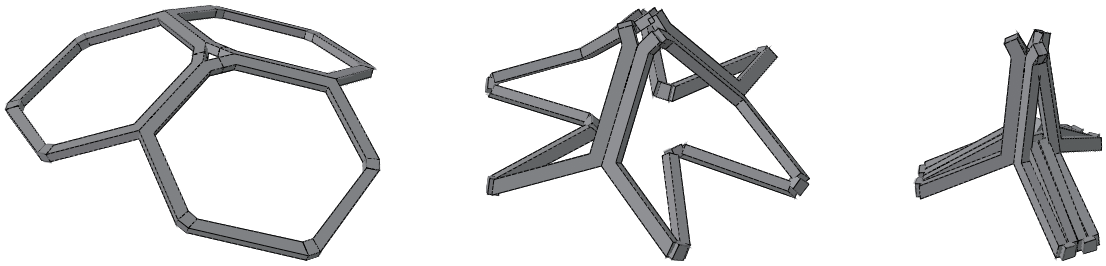

(a) (b) (c)

Figure 16. Three-fold symmetry tessellation concept with vertices located on the same sphere. b) and c) shows the half and fully folded state. This concept has a deployment ratio of 2.

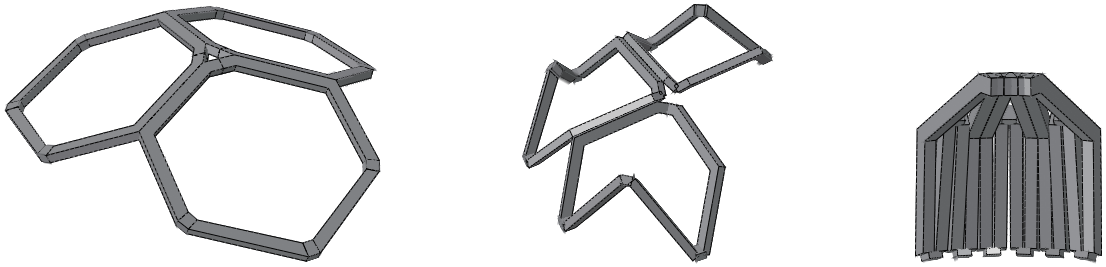

(a) (b) (c)

Figure 17. Three-fold symmetry tessellation concept with vertices located on the same spherical surface, one inter-module connection is detached. Additional rotation displacement control needs to be applied to the inter-module hinges to fold it compactly. b) and c) shows the half and fully folded state. This concept has a higher volumetric efficiency, i.e. volume of enclosing box of the folded mechanism.

B. Other Tessellation Concepts

Briefly shown here are two tessellation concepts based on the same modules and its adaptations, exploiting higher order of symmetry. These tessellations are generated through the same logic: articulating basic modules into multi-link spatial mechanism.

The mechanism in Figure 18 is adapted from the truncated icosahedron. Each basic module is a 4-link spherical mechanism forming a regular hexagon, but the hinges are placed on the edges instead of the vertices.

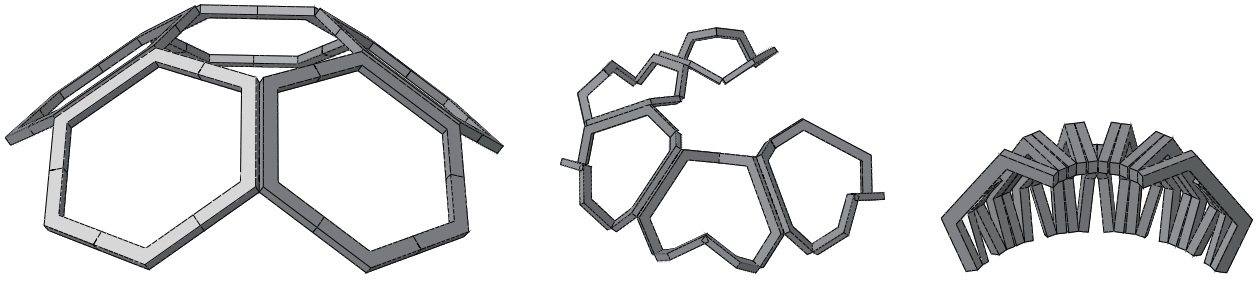

(a) (b) (c)

Figure 18. Tessellation concept based on part of truncated icosahedron, one inter-module connection is detached. The folding pattern is rotated 30° in this case, compared with figure 12. This concept has a deployment ratio of 1.6.

Employing higher order of symmetry will increase the degree of freedom of the tessellated mechanism, as shown by the concept in Figure 19. This concept deploys into a flat configuration, which employs the two basic modules shown in Figure 12 and Figure 18, respectively. It possesses 6-fold symmetry, and the inner ring is a 36-link spatial mechanism. Further analysis needs to be done to fully characterize the kinematic

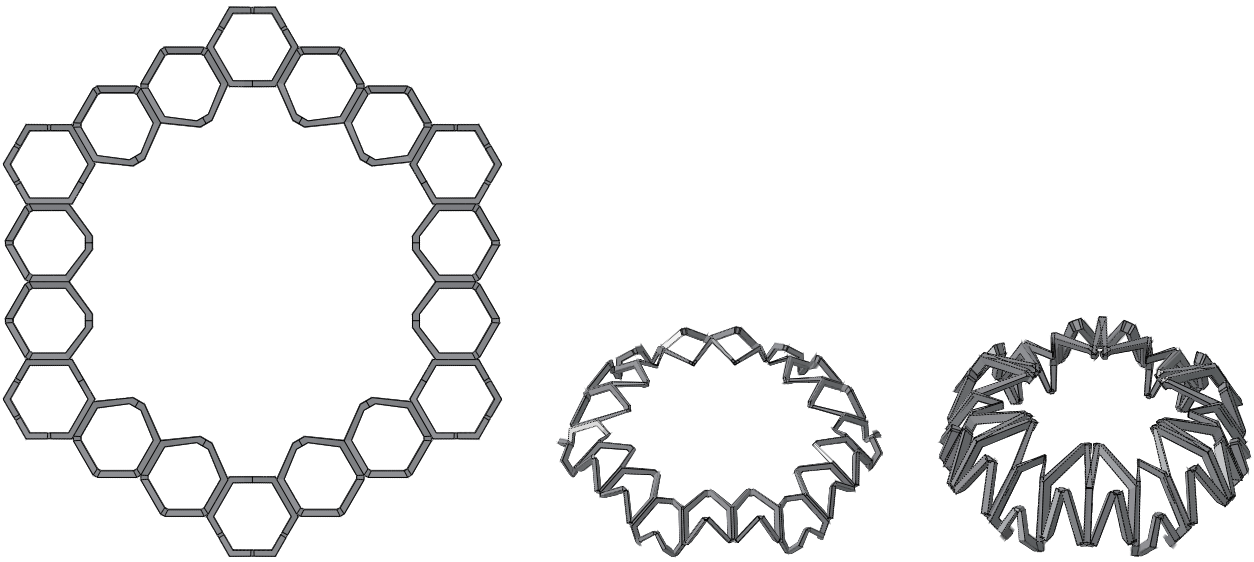

(a) (b) (c)

Figure 19. Tessellation ring concept based on two types of basic modules. This concept has a deployment ratio of 4.1.

characteristics of these multi-link spatial mechanisms.

VI. Modular Doubly-Curved Reflector with Edge Support

This section demonstrates the procedure to deploy a modular doubly curved reflector array. We first use piezoelectric actuation to introduce a spherical curvature into a thin flat substrate, then apply this approach to the tessellation concept from Section V to create a deployable, doubly curved reflector.

A. Introducing Non-Zero Gaussian Curvature to Flat Shell

It has been shown that unimorph structures, composed of thin substrates bonded with thin sheets of piezoceramic, can alter the surface shape locally. This technique has been used to create deformable mirrors which could compensate for incoming light's wavefront error.[15] Here we apply it to introduce a global curvature change to an initially flat substrate.

To create a thin, active unimorph shell, we bond a sheet of piezoceramic PZT-5A(actuator) to a thin aluminum plate. PZT-5A plates are commercially available from Piezo Systems Inc.. The piezoceramic sheet is cut into a circle of diameter 70 mm using a Universal® laser cutter, and the substrate is cut to a matching shape using a water jet cutter. To set a uniform bond line between the actuator and substrate, a low viscosity epoxy Epo-Tek® 301B is mixed with glass beads with diameter of 10 μm. A series of samples with varying thickness combination were manufactured and tested, as listed in Table 1.

Table 1. Unimorph samples with different thickness ratios and achievable radius of curvature.

Aluminum Substrate Thickness (μm)	Piezo Ceramic Thickness (μm)	Thickness Ratio	Achievable Radius of Curvature (m^{-1}) *
500	127	0.254	1.964
500	200	0.4	1.652
400	200	0.5	1.326

* Actuated under field strength 1 MV/m .

An electric field is applied across the thickness of the piezoceramic actuators. The actuators are pre-poled along the thickness direction, thus the applied electric field activates the d_{31} effect.[16] In all experiments the

field direction was aligned with the initial poling direction, which causes the actuators to shrink in-plane. Table 1 summarizes the thickness combinations that were investigated, and the achieved radii of curvature. These experiments demonstrated that by exploiting the thin substrate thickness and large blocking force, high d_{31} properties of the actuators, large curvature are attainable under moderate field strengths.

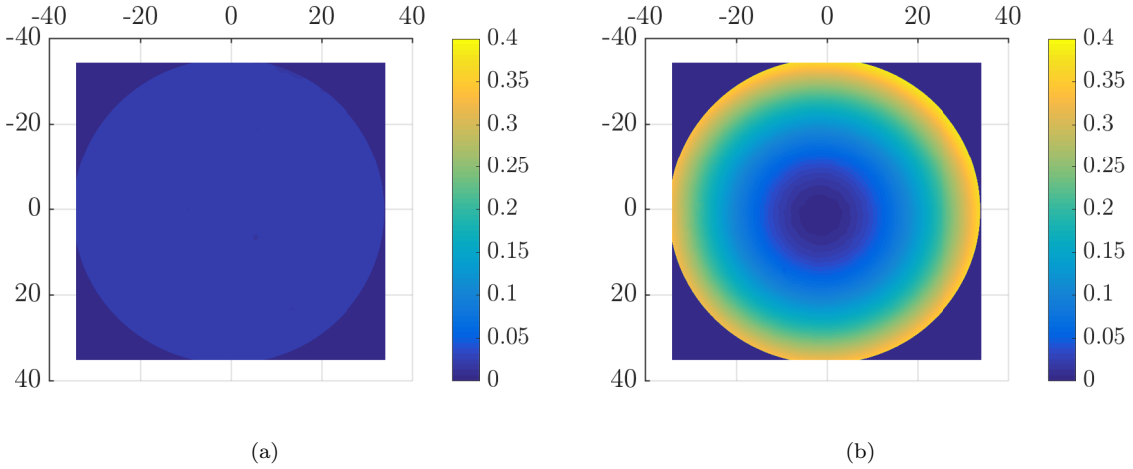

Figure 20. Measured out of plane displacement of unimorph sample a) before and b) after actuation under a field strength of 1 MV/m . Sample thickness ratio 0.4. Units in mm. Measurements taken with digital image correlation (DIC) system.

B. Curved Reflector Array Deployment and Actuation Concept

The concept shown in Figure 21 is based on the non-flat three-fold symmetry tessellation, also implementing the actuation scheme shown above. Bringing this reflector into operation involves two steps: deploying the support mechanism and actuation of the active shell. The deployment scheme for the mechanism can be based either on Figure 16 or on the detached version in Figure 17. After reaching the fully deployed configuration the hinges are locked and an electric field is applied to the unimorph reflector segments to achieve the final curved shape.

In this concept, the reflecting surface fills 70% of the total aperture area. It has an aperture size of 100 with a focal length of 140. This ratio could be changed over a wide range of choices, by altering the dihedral angle of the hexagons, essentially changing the internal angles of each deployable module.

VII. Conclusion

We have presented a novel deployable structure concept that allows packaging of a thin shell module whose edges are attached to a spatial mechanism. Steps for constructing compactly foldable spatial mechanisms from a rigid origami pattern were shown, then a thin origami shell with smooth folds was integrated with the mechanism to create a foldable surface module. Design and analysis of the concept were verified through a physical prototype. Multiple tessellation concepts have been proposed, both flat and curved after deployment, by linking the basic modules with revolute hinges. We have also demonstrated that a focal length can be introduced into initial flat mirror by means of thin, in-plane actuators.

References

[1]J. S. Archer, and W. B. Palmer. "Antenna technology for QUASAT application." *NASA Langley Research Center Large Space Antenna Systems Technol., p* 251-270 (1985).

[2]Dornier, "FIRST Technology study: multisurface control mechanism for a deployable antenna. " *Final report. Dornier Report RP-FA-D003* (1987).

[3]S. D. Guest, and S. Pellegrino. "A new concept for solid surface deployable antennas." *Acta Astronautica* 38.2: 103-113 (1996).

[4]M. S. Lake, J. E. Phelps, J. E. Dyer, D. A. Caudle, A. Tam, J. Escobedo, and E. P. Kasl. "A deployable primary mirror for space telescopes." *SPIE. Vol.* 3785 (1999).

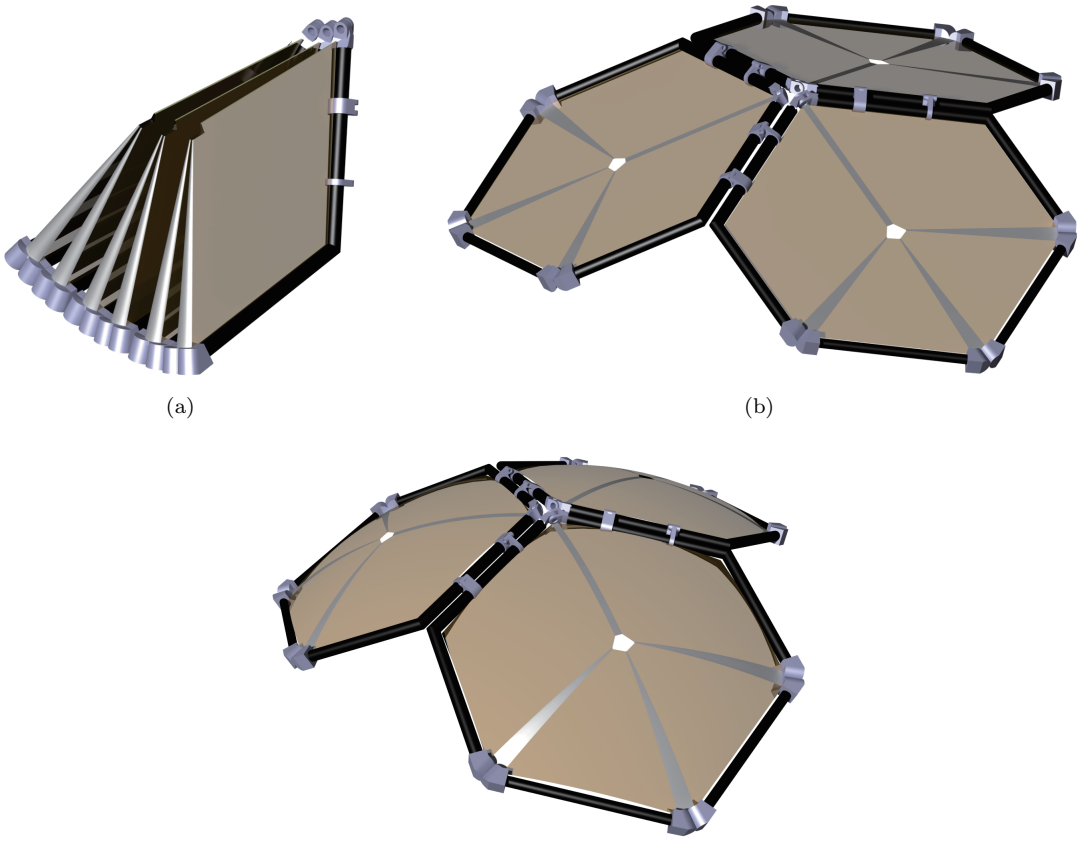

(a) (b) (c)

Figure 21. Concept of a modular deployable spherical reflector array, in pre and post actuation configuration.

[5]J. A. Champagne, S. M. Hansen, T. T. Newswander, and B. G. Crowther. "Cubesat image resolution capabilities with deployable optics and current imaging technology " (2014).

[6]N. Schwartz, D. Pearson, S. Todd, A. Vick, D. Lunney, and D. Macleod. "A Segmented Deployable Primary Mirror for Earth Observation from a CubeSat Platform" (2016).

[7]N. Lee, P. Backes, J. Burdic, S. Pellegrino, C. Fuller, K. Hogstrom, B. Kennedy, J. Kim, R. Mukherjee, C. Seubert, and Y. H. Wu. "Architecture for in-space robotic assembly of a modular space telescope." *Journal of Astronomical Telescopes, Instruments, and Systems* 2.4 : 041207-041207 (2016).

[8]J. J. Rey, A. Wirth, A. Jankevics, F. Landers, D. Rohweller, C. B. Chen, and A. Bronowicki. "A deployable, annular, 30m telescope, space-based observatory." *SPIE Astronomical Telescopes+ Instrumentation. International Society for Optics and Photonics* (2014).

[9]G. Durand, J. Amiaux, M. Sauvage, T. Martens, J. Austin, S. Chesne, C. Collette, C. Mayri, J. Pareschi, Y. Penfornis, G. Valsecchi, and U. Wittrock. "TALC a far-infrared 20m space telescope and the ELICSIR" consortium to reach TRL 3 (2016).

[10]T. Tachi. "Geometric considerations for the design of rigid origami structures." *Proceedings of the International Association for Shell and Spatial Structures (IASS) Symposium. Vol.* 12. (2010).

[11]Y. Chen, R. Peng, and Z. You. "Origami of thick panels." *Science* 349.6246: 396-400 (2015).

[12]T. J. Keil, and J. Banik. "Stowage and Deployment Strength of a Rollable Composite Shell Reflector." *Proc. of the 52nd AIAA/ASME/ASCE/AHS/ASC Structures, Structural Dynamics, and Materials Conference, Denver, CO.* (2011).

[13]R. C. Romeo, and R. N. Martin. "Unique space telescope concepts using CFRP composite thin-shelled mirrors and structures." *Optical Engineering+ Applications. International Society for Optics and Photonics* (2007).

[14]A. Meinel, M. Meinel, and R. C. Romeo. "Rollable Thin Shell Composite-Material Paraboloidal Mirrors" (2003).

[15]K. Patterson, N. Yamamoto, and S. Pellegrino. "Thin deformable mirrors for a reconfigurable space aperture." *53rd AIAA/ASME/ASCE/AHS/ASC Structures, Structural Dynamics and Materials Conference* (2012).

[16]J. Steeves, and S. Pellegrino. "Ultra-thin highly deformable composite mirrors." *54th AIAA Structures, Structural Dynamics, and Materials Conference* (2013).

[17]C. F. Lillie. "Large deployable telescopes for future space observatories." *Optics and Photonics 2005. International Society for Optics and Photonics* (2005).

[18]B. Audoly, and Y. Pomeau. **"Elasticity and geometry: from hair curls to the non-linear response of shells."** *Oxford University Press* (2010).

[19]K. Miura. "Method of packaging and deployment of large membranes in space." *The Institute of Space and Astronautical Science report* 618: 1-9 (1985).

[20]T. A. Evans, R. J. Lang, S. P. Magleby, and L. L. Howell. "Rigidly foldable origami gadgets and tessellations." *Royal Society open science* 2.9: 150067 (2015).

[21]J. J. Uicker, G. R. Pennock, and J. E. Shigley. **"Theory of machines and mechanisms. Vol. 1."** *New York, NY, USA: Oxford University Press* (2011).

[22]A. M. Watt, and S. Pellegrino. "Tape-spring rolling hinges." *Proceedings of the 36th Aerospace Mechanisms Symposium* (2002).

[23]P. A. Halverson. "Multi-stable compliant rolling-contact elements" (2007).

[24]H. Asada, and J.-J. E. Slotine. **"Robot analysis and control."** *John Wiley and Sons* (1986).

[25]H. M. Y. C. Mallikarachchi, and S. Pellegrino. "Quasi-static folding and deployment of ultra-thin composite structures." *Journal of Spacecraft and Rockets,* 48(1), 187-198 (2011).

[26]Metglas®, Inc. http://www.metglas.com (2016)

[27]Z. You, and Y. Chen. **"Motion structures."** *Taylor and Francis* (2011).